Iraqi Journal of Physics, 2025 *Vol. 23, No.3, PP.164-173*
https://doi.org/10.30723/ijp.v23i3.1398
P-ISSN: 2070-4003
E-ISSN: 2664-5548

Kinetic Study of Crystal Violet Dye Removal by Iron Oxide Nanoparticles Prepared by the Green Method

Takleef Dheyab Sallal[1] and Ahmed Mohammed Abbas[1*]
[1]*Department of Chemistry, Collage of Education for Pure Sciences (Ibn Al-Haitham), University of Baghdad, Baghdad, Iraq*
[*]Corresponding author: **ahmed.m.a@ihcoedu.uobaghdad.edu.iq**

Abstract
The green method was chosen for the preparation of nano iron oxide due to its simplicity, ease of preparation, and purity, compared to other methods. Nano iron oxide was made using a substance that causes precipitation and a coating from the alcoholic extract of orange leaves from Iraq. It was examined structurally and spectrally using several techniques, including X-ray diffraction, Fourier transform infrared spectroscopy, field-emission scanning microscopy (FESEM), energy-dispersive X-ray spectroscopy, and UV-Vis spectroscopy. The diagnosis proved that the nano iron oxide was successfully prepared in a spherical form and with an average size of 71.1 nm. The nano iron oxide particles were tested for their ability to remove crystal violet (CV) dye from an aqueous solution using the adsorption technique, achieving a removal percentage of 51% at 298K, with an adsorbent dose of 0.01 g, a contact time of 90 minutes, and an initial dye concentration of 11 mg/L. The adsorption process data were analyzed kinetically using kinetic models. It was found that the process follows the pseudo-second-order kinetic model, suggesting that the type of adsorption is chemical. The results indicate the potential use of nano iron oxide to protect the aquatic environment.

Article Info.

Keywords:
Fe_2O_3 NPs, Green Approach, Orange Leaf Ethanolic Extract, Kinetic of Adsorption, Crystal Violet Dye .

Article history:
Received: Nov. 13, 2024
Revised: Mar. 04, 2025
Accepted: Apr. 03, 2025
Published: Sep.01, 2025

1. Introduction
Nanotechnology and nanoscience are among the most important modern discoveries because they form the foundation of various areas of modern life. They are materials manufactured at a scale of 1-100 nanometers. Nanomaterials are distinguished from micromaterials by their surface effects of large surface area due to their size, a large number of particles per unit mass, and an increased percentage of atoms on the surface. The reduction in size led to dramatic changes in a number of physical and chemical properties of the material, such as reactivity, catalysis, melting point and conductivity [1, 2]. Several methods are employed to prepare nanomaterials, including chemical reduction, electro-optical deposition, co-deposition, spray thermal decomposition, hydrothermal, and sol-gel [3-5].

Recently, researchers have conducted an extensive study using magnetic nanoparticles (α-Fe_2O_3, γ-Fe_2O_3, Fe_3O_4, and FeO) in various general and biomedical applications [6-8]. Hematite (α-Fe_2O_3) is one of the most stable forms of iron oxide. Nano iron oxide particles have properties that make them effective and low-cost materials in several areas, including corrosion treatment, chemical stability, optics, magnetism, and biodegradability, providing ease and applicability in various modern applications. Applications of hematite nanoparticles include gas sensors, storage media, dyes, catalysis, corrosion treatment, solar energy conversion, and water purification [9- 11]. There are various methods for manufacturing iron nanoparticles, some are chemical using chemical solvents, which can produce toxic chemicals, making them dangerous and unsafe. Other methods are physical but expensive because they require high energy.

These reasons required the search for safe and environmentally friendly methods. This is achieved by the green methods, which use living materials in the preparation process [12]. Several previous studies have addressed the preparation of metal nanoparticles and their oxides using the green method through plant extracts and their parts (leaves and roots) as reducing agents [13-15].

Green synthesis of nanoparticles is preferable, environmentally friendly, and non-toxic. In this green synthesis route, biomolecules in the plant system can act as capping and reducing agents and increase the nanoparticles reduction rate and stability [16,17].

This study investigated the green production of α-Fe_2O_3 nanoparticles utilising ethanolic extract from Iraqi orange tree leaves. The synthesised iron oxide nanoparticles were characterised using several techniques (FT-IR, XRD, FESEM, EDX, and UV-Vis), and the samples were evaluated for their efficacy in clearing crystal violet (CV) dye from aqueous solutions.

2. Experimental Work

2.1. Materials and Reagents

Solutions and reagents were prepared according to analytical standards and without further purification. The chemicals used were supplied from Sigma-Aldrich, which were iron nitrate ($Fe(NO_3)_2.6H_2O$), ammonia hydroxide (NH_4OH), ethanol (C_2H_6O), and distilled water. All solutions were prepared with distilled water. Leaves of the orange plant were collected from the local area of Baghdad city in Iraq. Crystal violet dye (CV) ($C_{25}N_3H_{30}Cl$) was used for the adsorption tests.

2.2. Preparation of Leaves of Orange Plant Extract

Orange leaves were collected from one of the orchards of the Selman Pak area on the Tigris River in Baghdad Governorate. They were washed with distilled water several times to get rid of dust and other pollutants; the leaves were dried at room temperature for seven days without exposing them to sunlight. Orange extract was prepared in water by adding 200 mL of ethanol to 20 g of dried orange leaf powder in a 500 mL beaker with continuous stirring and heating at 60 °C for an hour. Then, the mixture was left for 24 hrs. The next day, the solution was filtered to obtain a clear brown bitter orange extract, which was then stored in special, tightly sealed bottles and refrigerated for further use.

2.3. Synthesis and Characterization of Iron Oxide Nanoparticles

10 mL of 0.01 M iron nitrate solution was placed in a beaker and stirred using a magnetic stirrer (hot plate and magnetic stirrer, LMS-100, Korea) for 30 minutes at 50 °C. The orange leaf extract as a reducing agent and a capping agent was gradually added until the mixture color changed to a dark brown and a precipitate appeared. Continuous stirring was maintained throughout this process to guarantee a uniform reaction. The resultant precipitate solution was centrifuged (Hermie Laborti Chink Type Z 200 A, 6000 rpm, Germany) at 5000 rpm for 20 minutes, followed by repeated washing with deionised water. The dried precipitate powder was subsequently heated at 700 °C for 8 hours in a furnace oven (Vindon LTD, Oldham, England) to yield dark red α-Fe_2O_3 nanoparticles [18].

The NPs were characterized with a field emission scanning electron microscope (FESEM, ZEISS model: Sigma VP-UK), X-ray diffractometer (Siemens model D500, Germany), and Fourier-transform infrared spectroscope (FTIR, IRPrestige-21Shimadzu, Japan) to determine the surface functional groups of the NPs, The optical transmission/absorption spectra of the particles in deionized water were recorded with a UV-Vis spectrometer (Shimadzu 1800, Japan) and energy disperse X-ray spectroscope (EDX, Oxford Instruments, UK).

2.4. Adsorption Experiments

The adsorption experiment was conducted by applying a batch system by mixing 0.01 g of Fe_2O_3 NPs with 10 ml of the violet dye (CV) solution of a concentration of 11 mg/L using a water bath shaker (Labtech, Sofor h Korea) at laboratory temperature, at 150 rpm agitation speed, and at range of agitation times (15, 30, 45, 60, 75, 90, and 120 min). Each sample was separated by centrifugation. Absorbance for each solution was measured by the UV-Vis spectrometer, and the amount of adsorbed dye and the percentage of adsorption (A%) were calculated through the following Eqs. (1 and 2), respectively [19–20]

$$\%A = \left(\frac{C_\circ - C_t}{C_\circ}\right) \times 100 \quad (\mathbf{1})$$

$$q_e = \left(\frac{C_\circ - C_t}{m}\right) V \quad (\mathbf{2})$$

where C_o and C_t are the CV dye concentrations at time t = zero and at t, respectively, V is the volume (L) of the CV dye solution, whereas m symbolizes the adsorbent weight (g).

3. Results and Discussion

3.1. Characterization of Fe_2O_3 NPs

3.1.1. XRD Analysis

Fig.1 shows the XRD pattern of iron oxide nanoparticles prepared by the ethanol extract of orange leaves within the range (2θ = 5-80°) containing strong and abundant peaks, reflecting the high crystallinity level of the resulting material. In addition, the diffraction peaks were identified at 2θ of 23.79°, 32.96°, 35.43°, 40.65°, 49.27°, 53.88°, and 63.82°, indexed as (10-2), (104), (110), (113), (20-4), (116), and (300), respectively, belonging to the magnetite nanoparticles (α-Fe_2O_3) according to standerd card (JCPDS 89-0599). No additional peaks were observed in the XRD pattern. Therefore, there were no additional levels in the XRD pattern compared to the standard card pattern., indicating the high purity of the α-Fe_2O_3 nanoparticles.

The average crystal size was calculated using the Debye-Scherrer formula [21]

$$S_{hkl} = \frac{k\lambda}{b\cos\theta} \quad (\mathbf{3})$$

where S_{hkl} is the average crystallite size (in nm), K is the Scherer constant of (0.89), λ is the incident X-ray wavelength, θ is the Bragg diffraction angle, and b is the Full Width at Half Maximum (FWHM), The average crystal size of the synthesized green hematite nanoparticles was about 71.1 nm [16,22].

3.1.2. FT-IR analysis

Fig.2 shows the FTIR spectrum displaying the presence of phytochemicals on the surface of α-Fe_2O_3 nanoparticles within the range 400-4000 cm^{-1}. A broad and weak peak at 3400 cm^{-1} is due to the stretching of the (OH) group. There is also a peak at 1544 cm^{-1} attributed to the stretching of the N=O group, while the peak 1120 cm^{-1} is attributed to the stretching of C-O. Therefore, all peaks can be attributed to the phytochemicals in the ethanolic extract, which are supposed to be responsible for the reduction of metal ions and their conversion to nanomaterials. The strong peaks around 472 and 538 cm^{-1}, which

indicate the presence of magnetite nanoparticles, can be confirmed by their corresponding to the Fe-O stretches of α-Fe_2O_3 [16, 22].

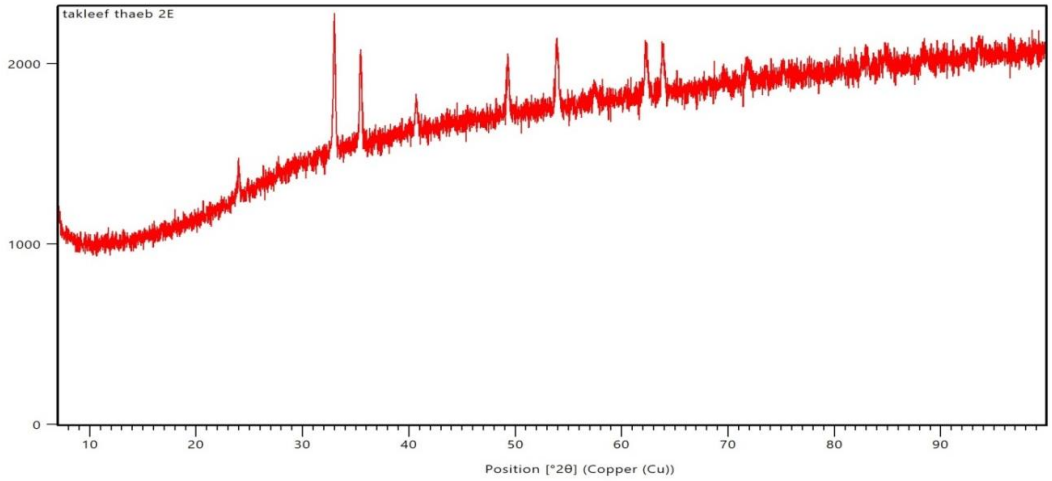

Figure 1: XRD patterns of iron oxide (a-Fe_2O_3) NPs.

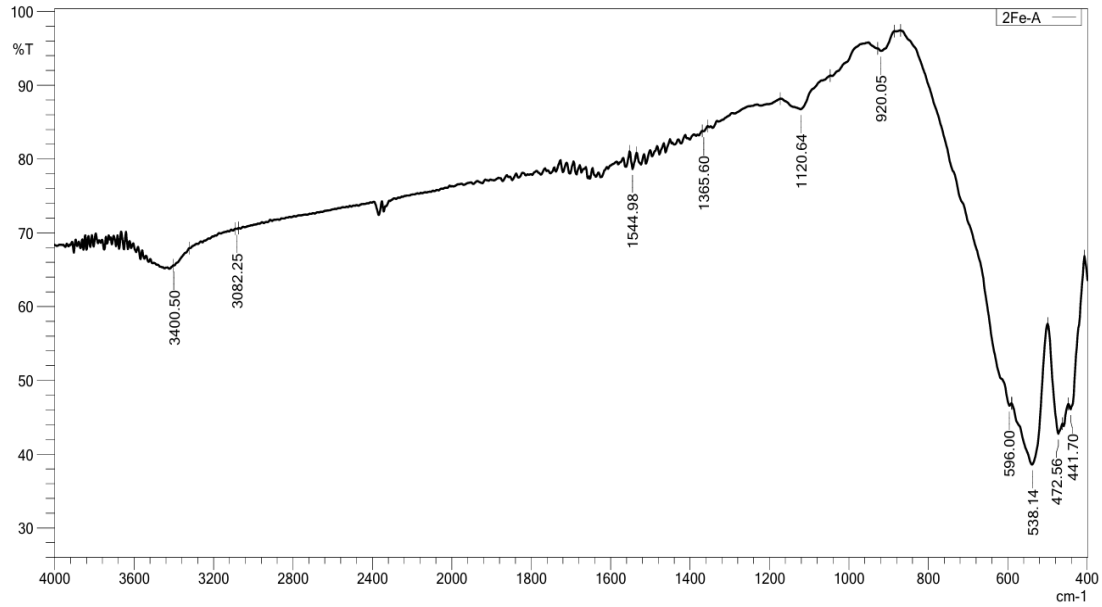

Figure 2: FT-IR Spectrum of iron oxide(a-Fe_2O_3) NPs.

3.1.3. FE-SEM analysis

FE-SEM technique is an important diagnostic tool for determining the morphology, agglomerations, shapes and sizes of nanomaterials. Fig. 3 shows a field-emitted scanning electron microscope image (at a magnification level of 100 nm) showing the surface morphology of the iron oxide nanoparticles synthesized by the orange leaf ethanolic extract (green method). The image showed the aggregation of particles in the form of homogeneous nano-spherical clusters of α-Fe_2O_3. The size of these particles in the form of clusters reached 113 nm, which is larger than the average size calculated according to the XRD data supporting single nanoparticle size [18].

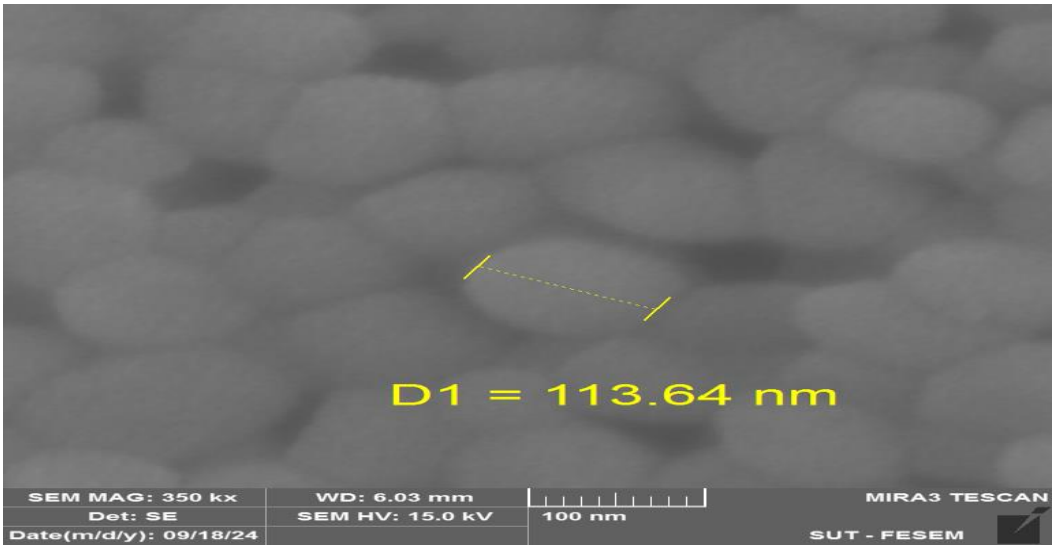

Figure 3: FE-SEM observation of iron oxide(a-Fe_2O_3) NPs.

3.1.4. EDX Analysis

The technique is one of the diagnostic tools for determining the purity and the percentage of chemical elements present in the composition of materials. Fig. 4 shows the energy dispersion X-ray (EDX) results of α-Fe_2O_3 nanoparticles that were manufactured in a green and environmentally friendly way orange leaf ethanolic extract. The percentages of the elements that make up the resulting nano-iron oxide were: 75.97 % Fe and 24.03 % O, indicating the success of preparing nano-iron oxide with high purity [22, 23, 24].

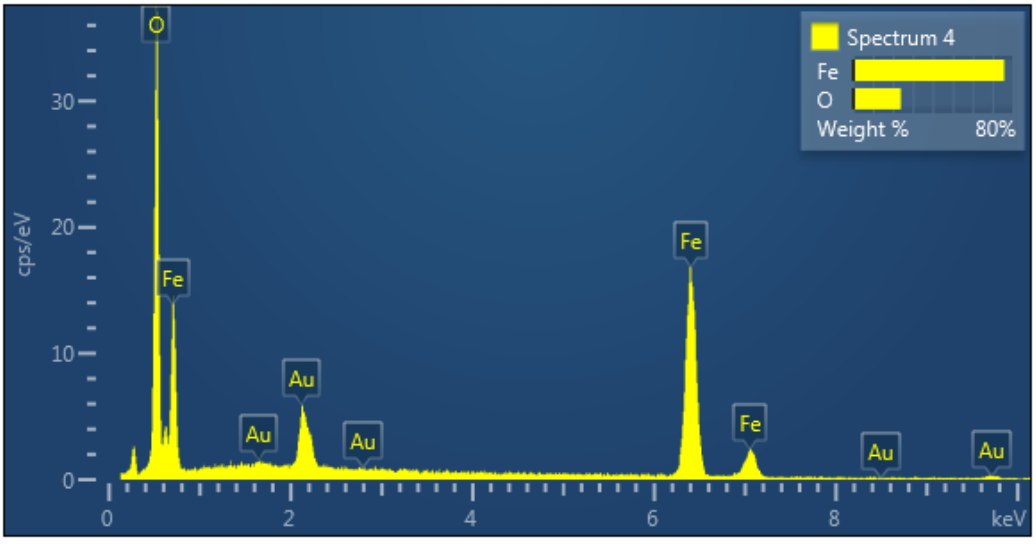

Figure 4: EDX Analysis of iron oxide(a-Fe_2O_3) NPs.

3.1.5. UV-Vis Analysis

Fig. 5 shows the UV-Vis absorption spectrum in the range 300–600 nm, which reflects the characteristic formation of nanoparticles during color change. The characteristic peak at 318 nm confirmed the formation of Fe_2O_3 nanoparticles [25].

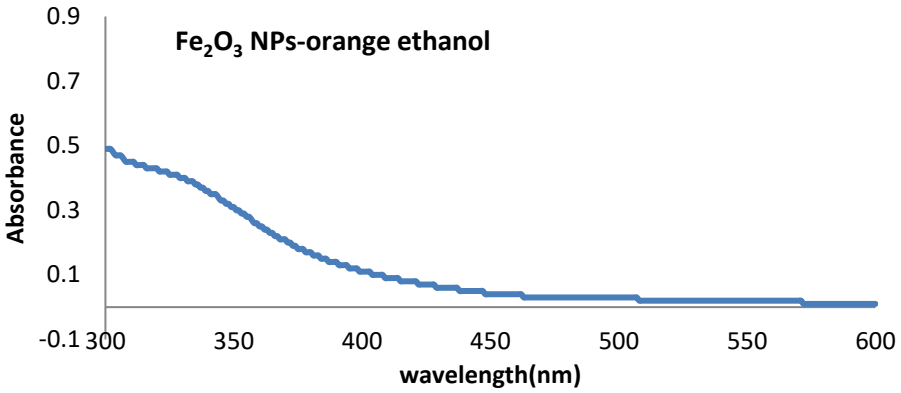

Figure 5: UV-Vis spectrum of iron oxide(a-Fe_2O_3) NPs.

3.2. Study of CV Dye Adsorption

The efficiency of CV dye adsorption by iron oxide nanoparticles was studied over agitation period of 15–180 min and at constant conditions, including pH 7, initial CV concentration of 11 mg/L, Fe_2O_3 nanoparticle weight of 0.01 g, and vibration speed of 150 rpm at 298 K. The amount of adsorbed CV dye increases with time and reaches equilibrium at about 90 min, after which the adsorption rate remains constant. This may indicate that the onset of the adsorption process of CV dye molecules is easy and fast through their attachment to the Fe_2O_3 nanoparticles that have a relatively large surface area. This process continues for at least 90 minutes after saturation of the unoccupied surface sites, with an adsorption efficiency of up to 51% (the adsorption amount of CV dye at equilibrium (qe) was 5.7 mg/g), as shown in Figs. 6 and 7 [26-28].

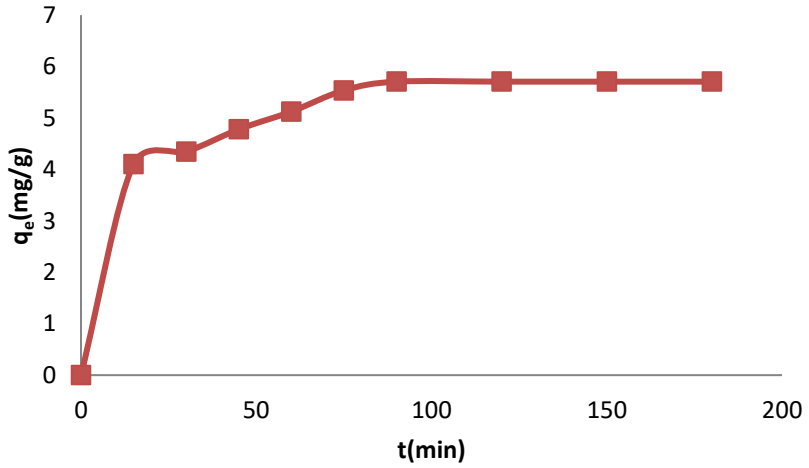

Figure 6: Effect of agitation time on the quantity adsorption of CV dye on Fe_2O_3 NPs.

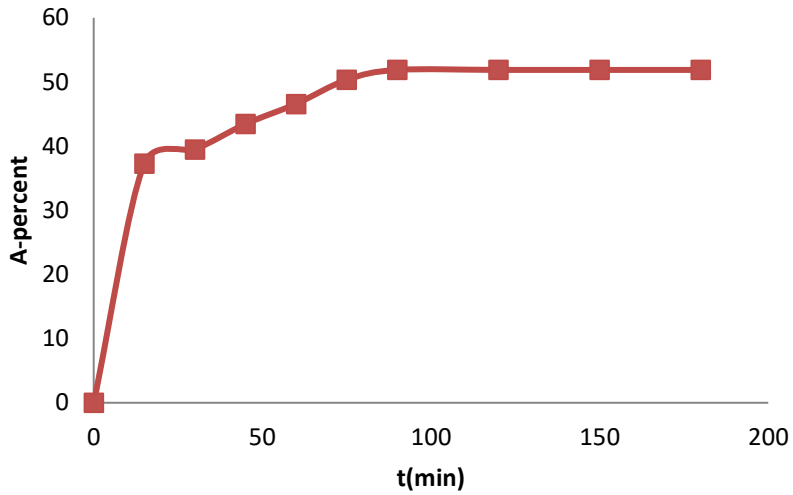

Figure 7: Effect of agitation time on the percent adsorption of CV dye on Fe_2O_3 NPs.

3.3.Kinetics of Adsorption

The experimental data were applied by kinetic models Pseudo-First-Order (PFO) and Pseudo-Second-Order (PSO). The linearized forms of (PFO) and (PSO) models have been applied using Eqs. (4 and 5), respectiveily [29, 30]

$$\mathrm{Ln}(q_e - q_t) = \mathrm{Ln}q_e - k_1 t \quad (4)$$

$$\frac{1}{q_e} = \frac{1}{k_2 q_e^2} + \frac{t}{q_e} \quad (5)$$

where q_t (at time t) and q_e (at equilibrium) are the quantities of CV dye adsorbed on the Fe_2O_3 NPs by unit (mg/g), k_1 (min^{-1}), k_2 ($g.mg^{-1}.min^{-1}$) are the rate constants of PFO and PSO, respectively. The linear forms of ln ($q_e - q_t$) versus (t) (Fig.8) and t/q_t versus t (Fig. 9) are employed to calculate k_1, q_e values for PFO and k_2, q_e values for PSO. The PFO and PSO constants for the CV dye adsorption process were recorded in Table 1. As noted from the table, the values of correlation coefficient R^2 for PSO were higher than those for PFO. Also, the values of q_e experimental ($q_{e\ exp}$) obtained using Eq.(2) and q_e calculated ($q_{e\ cal}$) by the graphs of Figs. 8, 9 were matched well using PSO kinetic models, suggesting that the mechanisms of adsorption are related to both adsorbent and adsorbate [31-33].

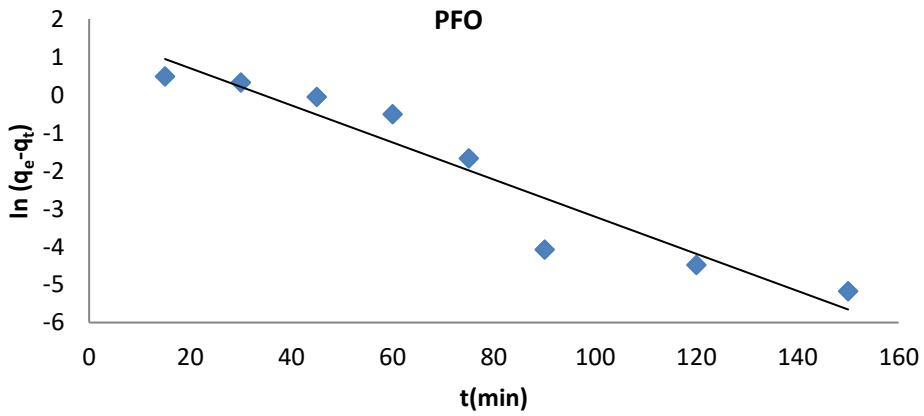

Figure 8: PFO linear form for CV dye adsorption of on Fe_2O_3 NPs.

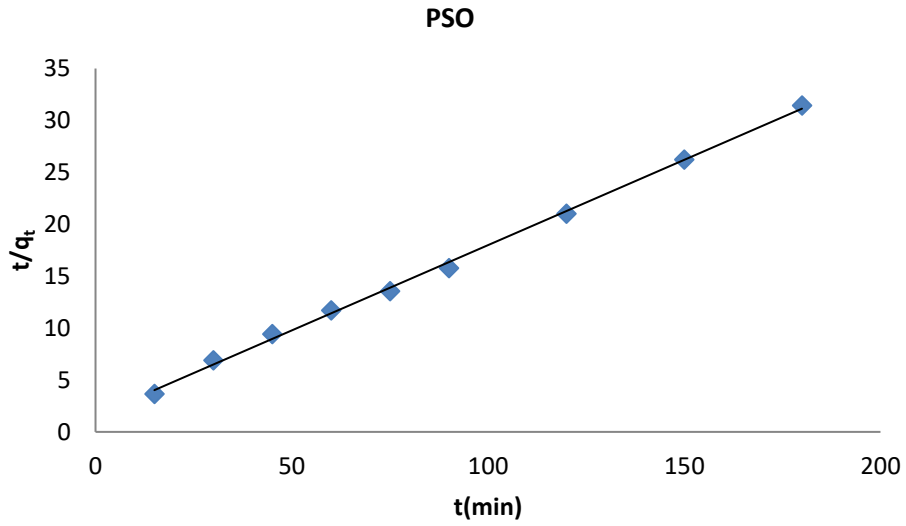

Figure 9: PSO linear form for CV dye adsorption of on Fe_2O_3 NPs.

Table 1: PFO and PSO kinetic constants for adsorption of CV dye on Fe_2O_3 NPs.

Surface	298 K			
	PFO			
	k_1 (min^{-1})	q_e(mg/g) (cal)	q_e(mg/g) (exp)	R^2
Fe_2O_3 NPs	0.0489	5.352	5.723	0.915
	PSO			
	k_2(g. mg^{-1} .min^{-1})	q_e(mg/g) (cal)	q_e(mg/g) (exp)	R^2
	0.0173	6.086	5.723	0.998

4. Conclusions

This study used the ethanolic extract of orange leaves to synthesize nano-iron oxide in the form of medium-sized spherical particles (according to FESEM data) with an average size of 71.1 nm (according to XRD data) and of high purity (according to EDX data) with a perfect match of the dominant peaks with the data (FT-IR and UV-vis) of previous studies, which reflects the efficiency of the green method in preparing nano-iron oxide. The nano-iron oxide was tested and gave good efficiency in removing the purple crystalline dye. It was also found that the experimental results of the adsorption follow the second-order kinetic model, indicating that the adsorption type is chemical. As a result of the above, this may open a horizon in preparing nanomaterials and applying them in the purification field.

Acknowledgements

The authors thank the Department of Chemistry, Faculty of Education for Pure Sciences (Ibn Al-Haitham), University of Baghdad for its support in approving this study through laboratories, devices, tools, measurements and chemical materials.

Conflict of Interest

Authors declare that they have no conflict of interest.

References

1. E. Roduner Chem Soc Rev., **35**, 583 (2006). https://doi.org/10.1039/B502142C.
2. A. S. Tawfik, Environ. Technol. Innov., **20**, 101067 (2020). https://doi.org/10.1016/j.eti.2020.101067.
3. S. Veeranna, A., Burhanuddin, S. Khanum, S. L. Narayan, and K. Pratima, K. Res. J. Biotechnol., **8**, 11 (2013). https://doi.org/10.1186/s11671-019-3244-z.
4. A. Lassoued, B. Dkhil, A. Gadri, and S. Ammar, Results Phys., **7**, 3007 (2017). https://doi.org/10.1016/j.rinp.2017.07.066.
5. A. M. Abbas, F. H. Abdulrazzak, W. J. Sabbar, and R. A. S. Faraj, J. Mater. Environ. Sci, 11, 2007 (2020).
6. A. Ali, H. Zafar, M. Zia, I. ul Haq, A. R. Phull, J. S. Ali, and A. Hussain, Nanotechnol Sci Appl, 49 (2016). https://doi.org/10.2147/NSA.S99986.
7. T.S. Rasha, E. A. Dunya, Iraqi J. Sci, **64**, 4679 (2023). https://doi.org/10.24996/ijs.2023.64.8.5.
8. A. S. Teja, and P. Y. Koh, Prog. Cryst. Growth Charact. Mater, **55**, 22 (2009). https://doi.org/10.1016/j.pcrysgrow.2008.08.003.
9. K. K. Kefeni, T. A. Msagati, T. T. Nkambule, and B. B. Mamba, J. Environ. Chem. Eng., **6**, 1865 (2018). https://doi.org/10.1016/j.jece.2018.02.037.
10. C. Wu, P. Yin, X. Zhu, C. OuYang, and Y. Xie, J. Phys. Chem. B., **110**, 17806 (2006). https://doi.org/10.1021/jp0633906.
11. N.Hasan, Z. Guo, and H. F. Wu, Anal Bioanal Chem., **408**, 6269 (2016). https://doi.org/10.1007/s00216-016-9730-6.
12. L. K. Ruddaraju, S. V. N. Pammi, G. Sankar Guntuku,V. S. Padavala, and V. R. M. Kolapalli, Asian J. Pharm. Sci., **15**, 42 (2020). https://doi.org/10.1016/j.ajps.2019.03.002.
13. F. H. Abdulrazzak, A. M. Abass, A. F. Alkaim, and F. H. Hussein, NeuroQuantology, **18**, 5 (2020).
14. L. K. Ruddaraju, S. V. N. Pammi, P. V. K. Pallela, V. S. Padavala, and V. R. M. Kolapalli, Mater. Sci. Eng. C, **103**, 109756 (2019). https://doi.org/10.1016/j.msec.2019.109756.
15. P. N. V. K. Pallela, S. Ummey, L. K. Ruddaraju, P. Kollu, S. Khan, and S. V. N. Pammi, SN APPL SCI. **1**, 1 (2019). https://doi.org/10.1007/s42452-019-0449-9.
16. P. N. V. K. Pallela, S. Ummey, L. K. Ruddaraju, S. Gadi, C. S. Cherukuri, S. Barla, and S. V. N. Pammi, Heliyon, **5**, 11 (2019). https://doi.org/10.1016/j.heliyon.2019.e02765.
17. S. Hemalatha, and R.S. Venkatesan, Ann Rom Soc Cell Biol, 1683 (2021). http://annalsofrscb.ro/index.php/journal/article/view/1614.
18. P. R. S. Baabu, H. K. Kumar, M. B. Gumpu, J. BabuK , A. J. Kulandaisamy, and J. B. B. Rayappan, Materials, **16**, 59 (2022); https://doi.org/10.3390/ma16010059.
19. M. A.Jasim, A. M. Abbas, and L. M. Radhi, AIP Conf. Proc. **2372**, 1 (2021). https://doi.org/10.1063/5.0068746.
20. A. M. Abbas, Y. I. Mohammed, and T. A. Himdan, Ibn al-Haitham J. Pure Appl. Sci., **28**, 52 (2017). https://jih.uobaghdad.edu.iq/index.php/j/article/view/177/146.
21. I. M. Radhi, S. S. Abd, R. A. S. Faraj, A. M. Abbas, and T. A. Himdan, Mong. J. Chem., **25**, 19 (2024). https://doi.org/10.5564/mjc.v25i52.3450.
22. A. Rufus, N. Sreeju, and D. Philip, RSC Adv, **6**, 94206 (2016). https://doi.org/10.1039/C6RA20240C.
23. D. Y. Yass, and A. M. Abbas, Her. Bauman Mosc. State Tech. Univ. Ser. Nat. Sci., **115**, 121 (2024). https://doi.org/10.1016/j.eti.2020.101072.
24. A. M. Abbas, F. H. Abdulrazzak, I. M. RadhI, A. L. AbdulLatif, T. A. Himdan, and F. H. Hussein, J. Phys. Conf. Ser., **1660**, 012022 (2020). https://doi.org/10.1088/1742-6596/1660/1/012022.
25. W. Sabbar, and A. M. Abbas, Ann Rom Soc Cell Biol, **25**, 5706 (2021). http://annalsofrscb.ro/index.php/journal/article/view/6587.
26. A. M. Abbas, S.S. Abd, and T. Abdulhadi Himdan, Ibn al-Haitham j. Pure Appl. Sci., **31**, 58 (2018). https://doi.org/10.30526/31.1.1853.
27. A. M. Abbas, Y. I. Mohammed, and T. A. Himdan, Ibn al-Haitham J. Pure Appl. Sci., **28**, 54 (2017). https://jih.uobaghdad.edu.iq/index.php/j/article/view/190/159.
28. M. Benjelloun, Y. Miyah, G. A. Evrendilek, F. Zerrouq, and S. Lairini, Arab. J. Chem., **14**, 103031 (2021). https://doi.org/10.1016/j.arabjc.2021.103031.
29. S. Bentahar, A. Dbik, M. El Khomri, N. El Messaoudi, B. Bakiz, and A. Lacherai, Sci. Stud. Res., Chem. Chem, **17**, 295 (2016).
30. S. S. Abd, and A. M. Abbas, Nat. Environ. Pollut. Technol, **18**, 863 (2019).
31. R. A. S. Faraj, and A. M. Abbas, J. Phys. Conf. Ser., **1879**, 022076 (2021). https://doi.org/10.1088/1742-6596/1879/2/022076.

32. H. Jawad, and A. M. Abbas, Ibn Al-Haitham J. Pure Appl. Sci, **34**, 19 (2021). https://doi.org/10.30526/34.1.2550.
33. S. A. Saed, and D. E. AL-Mammar, Iraqi J. Sci., 1761 (2021). https://doi.org/10.24996/ijs.2021.62.6.2.

دراسة حركية لازالة صبغة البلورات البنفسجية بواسطة الدقائق النانوية لاوكسيد الحديد المحضرة بالطريقة الخضراء

تكليف ذياب صلال[1] واحمد محمد عباس[1]
[1] قسم الكيمياء، كلية التربية للعلوم الصرفة (ابن الهيثم)، جامعة بغداد، بغداد، العراق

الخلاصة
اختيرت الطريقة الخضراء لتحضير أكسيد الحديد النانوي نظرًا لبساطتها وسهولة تحضيرها ونقائها مقارنةً بالطرق الأخرى. صُنع أكسيد الحديد النانوي باستخدام مادة تُسبب الترسيب، وطلاء من المستخلص الكحولي لأوراق البرتقال العراقية. وخضع لفحص هيكلي وطيفيّ باستخدام عدة تقنيات، منها حيود الأشعة السينية، ومطيافية تحويل فورييه للأشعة تحت الحمراء، ومجهر مسح الانبعاث الميداني (FESEM)، ومطيافية الأشعة السينية المشتتة للطاقة، ومطيافية الأشعة فوق البنفسجية والمرئية. وأثبت التشخيص نجاح تحضير أكسيد الحديد النانوي بشكل كروي، وبمتوسط حجم 71.1 نانومتر. تم اختبار قدرة جزيئات أكسيد الحديد النانوية على إزالة صبغة الكريستال البنفسجي (CV) من محلول مائي باستخدام تقنية الامتزاز، محققةً نسبة إزالة بلغت 51% عند درجة حرارة 298 كلفن، بجرعة ماصة مقدارها 0.01 غرام، وزمن تلامس 90 دقيقة، وتركيز أولي للصبغة مقداره 11 ملغم/لتر. حُللت بيانات عملية الامتزاز حركيًا باستخدام نماذج حركية. وتبين أن العملية تتبع نموذجًا حركيًا شبه ثانٍ، مما يشير إلى أن نوع الامتزاز كيميائي. وتشير النتائج إلى إمكانية استخدام أكسيد الحديد النانوي لحماية البيئة المائية.

الكلمات المفتاحيه: جسيمات نانوية من أكسيد الحديد، المنهجية الخضراء، المستخلص الايثانولي لاوراق البرتقال، حركيات الامتزاز، صبغة البلورات البنفسجية.